Chin.J.Geochem.(2014)33:077–085
DOI: 10.1007/s11631-014-0661-7

Carbon and oxygen isotopes suggesting deep-water basin deposition associated with hydrothermal events (Shangsi Section, Northwest Sichuan Basin-South China)

CHEN Hui[1*], XIE Xi'nong[1], MAO Kainan[1], and HUANG Junhua[2]

[1] *Key Laboratory of Tectonics and Petroleum Resources of Ministry of Education, Faculty of Resources, China University of Geosciences, Wuhan 430074, China*

[2] *State Key Laboratory of Geological Processes and Mineral Resources, Faculty of Geosciences, China University of Geosciences, Wuhan 430074, China*

[*] *Corresponding author, E-mail: hui.chen.cug@gmail.com*

Received June 19, 2013; accepted August 10, 2013

Abstract Carbon and oxygen isotope records for Shangsi Section in Northwest Sichuan Basin, South China can help investigating depositional environments and processes, including the burial rate and possible contribution of hydrothermal events. Samples from the lower Chihsian Formation show $\delta^{13}C_{PDB}$ and $\delta^{18}O_{PDB}$ values close to those of typical marine limestone. However, the overlying Permian middle-upper Chihsian, Wujiaping, and Maokou Formation samples reveal negative $\delta^{18}O_{SMOW}$ values and strong positive $\delta^{13}C_{PDB}$ values. These indicate high biological productivity and rapid burial of organic carbon. Samples from the Dalong Formation present both negative $\delta^{13}C_{PDB}$ and negative $\delta^{18}O_{PDB}$ values, which are quite different from the underlying Permian strata. These abnormal carbon and oxygen isotope characteristics in the Dalong Formation may suggest that hydrothermal processes contributed to deposition.

Key words carbon isotope; oxygen isotope; hydrothermal process

1 Introduction

Along with organic and carbonate carbon pools, hydrothermal deposition processes of igneous/ magmatic mantle systems could play an important role influencing carbon isotope (as well as oxygen isotope) changes (Hoefs, 1997). Stable isotope studies on carbonate rocks may provide valuable information concerning the precipitation of ore and gangue carbonates, the chemical evolution of mineralising fluids, and the processes of fluid-mixing and/or fluid-rock interaction (Ghazban et al., 1991; Huang Zhilong et al., 2010; Tao Shizhen et al., 2012).

Considerable work performed by the oil and gas exploration industry indicates that the Permian strata in the Sichuan Basin, Southwest China contain important source rocks for gas (Wang Yigang et al., 2006; Xu Sihuang and Wantney, 2007; Hao Fang et al., 2008; Ma Yongsheng, 2008; Zhang Qu et al., 2008; Zhou Huayao et al., 2008; Zhu Yangming et al., 2008; Zhu Guangyou et al., 2011). This finding has stimulated intense interest in studying the related depositional environments of the Permian strata in the Sichuan Basin. Organic and inorganic geochemical studies have been used to track paleo-environmental events and to reconstruct paleo-depositional conditions (Ma Zhixin et al., 2008; Ma Zhongwu et al., 2008; Ruan Xiaoyan et al., 2008; Xie Xi'nong et al., 2008; Zhou Lian et al., 2008). Bai Xiao et al. (2008) reported the carbon and oxygen isotope records of the Permian Shangsi Section in the Northwest Sichuan Basin and preliminarily discussed the possible indications of anoxic depositional environment, upwelling, and volcanic events. Lai Xulong et al. (2008) and Li Pengwei et al. (2009) focused on the P-T (Permian-Triassic) boundary extinction event with carbon-oxygen-sulphur (C-O-S) isotopic geochemistry of the Shangsi Section. Hu Guoyi et al. (2012) used carbon isotopes to distinguish the genetic types of coal-derived gas in the Sichuan Basin. Zhang Bing et al. (2012) studied carbon, oxygen, and strontium stable isotopes and discussed the relationship between dolomite reservoirs and diagenetic systems of the Changxing Formation in the eastern Sichuan Basin. However, isotope analysis is seldom used to infer paleo-depositional/diagenetic processes in this region.

This study investigates the carbon and oxygen isotope records of the Permian Shangsi Section, initially reported by Bai Xiao et al. (2008), in the Northwest Sichuan Basin. The results have been found comparable to the quantitative model of measured C and O isotope co-variation addressed by Spangenberg et al. (1996). This model could be used to characterise geochemical mixing processes and indicate temperature and pressure changes during possible hydrothermal events.

2 Geological setting

The Shangsi Section is located in the Guangyuan area in Northeast Sichuan Province, South China (Fig. 1A, B). Tectonically, it belongs to the Longmen Mountain fold belt in the northern Yangtze block (Fig. 1C). The Permian strata exposed in the Shangsi Section include, from bottom to top, the Liangshan, Chihsian, Maokou, Wujiaping, and Dalong formations, with a total thickness of ~380 m (Fig. 2). The excellent exposure of the Shangsi Section makes it one of four candidates for the Global Boundary Stratotype Sections and Points (GSSPs) for the P/T boundary strata in China (Yin Hongfu et al., 2001).

The Liangshan Formation consists primarily of aluminous layers, with a thickness of ~2 m. The Chihsian Formation (~230 m in thickness) contains bioclastic/nodular/laminated limestone, dolomite, bioclastic wackstone/packstone, carbonaceous shale, and siliceous mudstone or siliceous nodules, indicating an open or restricted carbonate platform. The lower-middle Maokou Formation contains limestone and bioclastic packstone with irregular concretions, whereas the upper formation contains interbeds of limestone, calcareous mudstone, and thinly bedded chert or siliceous rocks, with a total thickness of ~66 m, likely deposited in a neritic and open carbonate platform. Originating from the Dongwu Movement in the southwestern margin of the Upper Yangtze Platform, a regional unconformity occurs between the Maokou and Wujiaping formations, which has been recognised as an aluminous layer at the bottom of the Wujiaping Formation. The Wujiaping deposit (~55 m in thickness) is composed of bioclastic limestone with striped siliceous rocks or concretions that are formed in littoral and open carbonate platform environments. The Dalong Formation (~40 m in thickness) is dominated by interbedded siliceous rocks and calcareous mudstone with little limestone, indicating deeper basin floor environments.

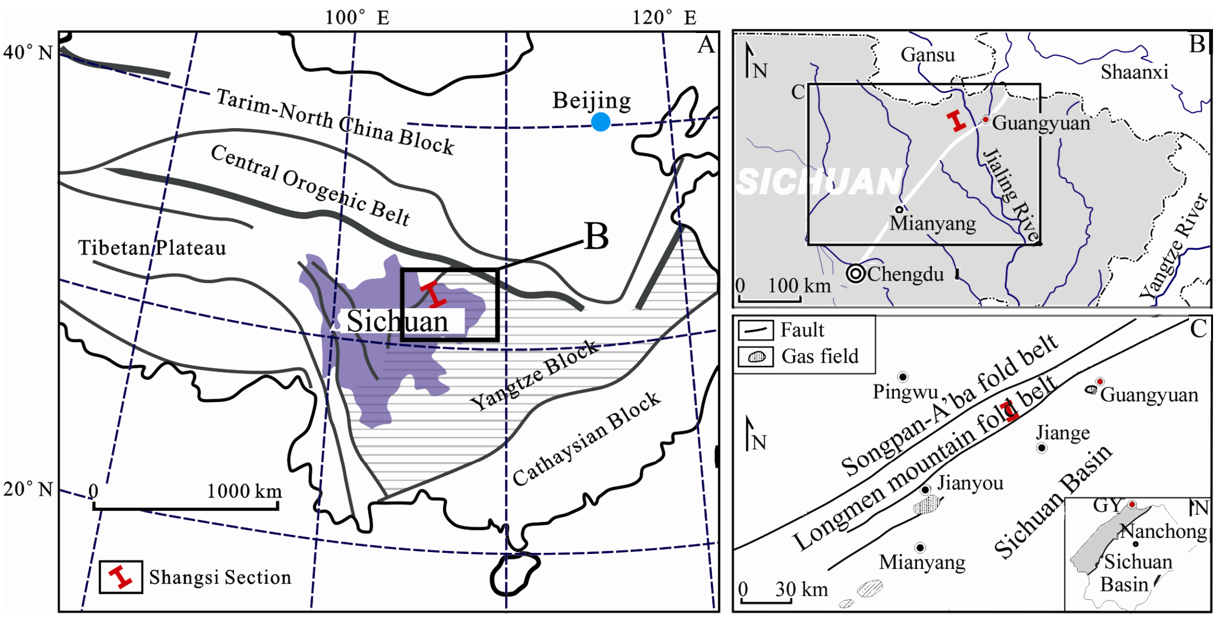

Fig. 1. (A) Sketch map of China showing position of Sichuan Province (modified from Qi Liang et al., 2008); (B) Location map of the Shangsi Section (modified from Isozaki et al., 2007); (C) Regional structure information of the sampling Shangsi section in the northwestern Sichuan Basin, Southwestern China (modified from Rao Dan et al., 2008; Yang Rongjun et al., 2009).

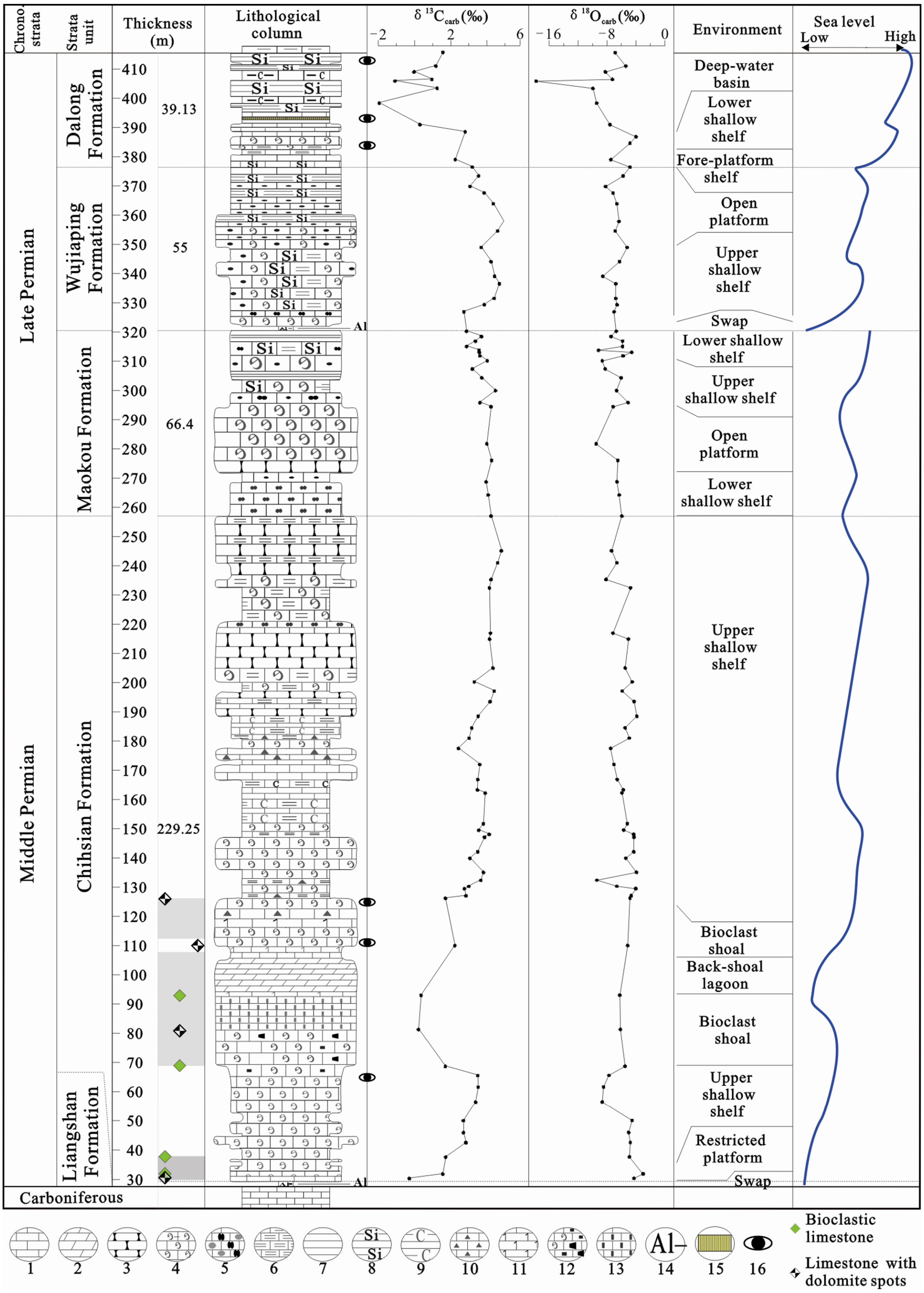

Fig. 2. Lithological column, containing $\delta^{13}C_{PDB}$, $\delta^{18}O_{PDB}$, sedimentary facies and sea level fluctuations (modified form Xie Xi'nong et al., 2008; Yan Jiaxin et al., 2008) of the Shangsi Section in the Northwest Sichuan Basin, Southwest China. Lithology symbols: 1. limestone; 2. dolomite; 3. nodular limestone; 4. bioclastic limestone; 5. limestone with cherts; 6. laminated limestone; 7. shale; 8. siliceous shale; 9. carbonaceous shale; 10. limestone containing asphalt; 11. dolomitised limestone; 12. limestone with dolomite spots; 13. limestone packed with calcite; 14. aluminous layer; 15. volcanic ashes; 16. positions of photographs shown in Fig. 3. Samples of bioclastic limestone (green diamonds) and limestone with dolomite spots (black and white diamonds) are referred in Figs. 3 and 4.

3 Analysis methods

Eighty-four samples collected from different lithologies in the Shangsi Section were used for carbon and oxygen isotopic analysis. Before measuring the carbon isotopes, samples were crushed to smaller than 100-mesh. Then, they were allowed to react with 100% H_3PO_4 under vacuum for more than 24-hour to produce CO_2. The CO_2 collected from this procedure was introduced into a Finigan MAT 251 mass spectrometer for measuring the ratios of $^{13}C/^{12}C$ and $^{18}O/^{16}O$. All of the carbon and oxygen isotope ratios obtained are reported in the δ notation relative to the international PDB standard and with precision better than ±0.1‰ for $\delta^{13}C$ and ±0.2‰ for $\delta^{18}O$. This analysis was conducted at the State Key Laboratory of Geological Processes and Mineral Resources, China University of Geosciences (Wuhan) (Bai Xiao et al., 2008). For the conversion from $\delta^{18}O$ (‰, PDB) to $\delta^{18}O$ (‰, SMOW), we use the following formula: $\delta^{18}O_{SMOW}$ (‰)=1.03091×$\delta^{18}O_{PDB}$+30.91 (Coplen et al., 1983).

4 Results and discussion

4.1 Carbon and oxygen isotope results

Carbon and oxygen isotope results from the Shangsi Section rocks are presented in Table 1, with outcrop photographs of strata from the Chihsian Formation (Layers 31, 44 and 49) and the Dalong Formation (Layers 135–140, 145–149 and 159–164) shown in Fig. 3A–F (see the positions of photographs in Fig. 2).

4.1.1 Samples from the Chihsian Formation

Forty-four samples were collected from the Chihsian Formation: 14 bioclastic limestone samples show $\delta^{13}C_{PDB}$= +0.4‰ to +3.9‰ and $\delta^{18}O_{SMOW}$= +22.0‰ to +27.8‰, with average values of +2.7‰ and +25.1‰, respectively; 12 samples from the host rock of limestone interbedded with laminated limestone show $\delta^{13}C_{PDB}$ = +2.8‰ to +4.8‰ and $\delta^{18}O_{SMOW}$ = +21.2‰ to +26.9‰, with average values of +4.0‰ and +24.7‰, respectively; eight limestone samples show $\delta^{13}C_{PDB}$= +3.5‰ to +4.3‰ and $\delta^{18}O_{SMOW}$= +23.5‰ to +26.5‰, with average values of +3.9‰ and +25.0‰, respectively; four samples from the host rock of limestone with dolomite spots show $\delta^{13}C_{PDB}$= –0.3‰ to +2.2‰ and $\delta^{18}O_{SMOW}$= +24.6‰ to +26.5‰, with average values of +1.0‰ and +25.7‰, respectively; three samples from the host rock of limestone containing asphaltene show $\delta^{13}C_{PDB}$= +2.4‰ to +3.0‰ and $\delta^{18}O_{SMOW}$= +23.2‰ to +26.8‰, with average values of +2.7‰ and +25.3‰, respectively; and three samples from the host rock of limestone interbedded with shale show $\delta^{13}C_{PDB}$= +3.2‰ to +3.6‰ and $\delta^{18}O_{SMOW}$= +25.0‰ to +26.9‰, with average values of +3.4‰ and +25.7‰, respectively.

4.1.2 Samples from the Maokou Formation

Seventeen samples were collected from the Maokou Formation: Eight samples from the host rock of limestone interbedded with siliceous bands and carbonaceous shale show $\delta^{13}C_{PDB}$= +2.9‰ to +4.0‰ and $\delta^{18}O_{SMOW}$= +21.5‰ to +26.2‰, with average values of +3.5‰ and +23.6‰, respectively; four limestone samples show $\delta^{13}C_{PDB}$= +3.6‰ to +4.3‰ and $\delta^{18}O_{SMOW}$= +21.1‰ to +25.7‰, with average values of +4.0‰ and +23.6‰, respectively; three samples from the host rock of limestone interbedded with cherts show $\delta^{13}C_{PDB}$= +4.0‰ to +4.5‰ and $\delta^{18}O_{SMOW}$ = +24.0‰ to +24.4‰, with average values of +4.2‰ and +24.2‰, respectively; and two samples from the host rock of limestone interbedded with carbonaceous shale show $\delta^{13}C_{PDB}$= +2.9‰ to +3.4‰ and $\delta^{18}O_{SMOW}$= +24.88‰ to +24.89‰, with average values of +3.1‰ and +24.88‰, respectively.

4.1.3 Samples from the Wujiaping Formation

Fourteen samples were collected from the Wujiaping Formation: Seven samples from the host rock of limestone interbedded with cherts show $\delta^{13}C_{PDB}$= +2.7‰ to +4.4‰ and $\delta^{18}O_{SMOW}$= +22.1‰ to +25.9‰, with average values of +3.6‰ and +23.9‰, respectively, and seven samples from the host rock of limestone interbedded with siliceous bands show $\delta^{13}C_{PDB}$ = +3.5‰ to +4.9‰ and $\delta^{18}O_{SMOW}$= +23.8‰ to +25.0‰, with average values of +4.3‰ and +24.3‰, respectively.

4.1.4 Samples from the Dalong Formation

Nine samples were brought from the Dalong Formation: Seven siliceous rock samples show $\delta^{13}C_{PDB}$= –2.0‰ to +2.3‰ and $\delta^{18}O_{SMOW}$= +12.6‰ to +25.4‰, with average values of +0.6‰ and +21.5‰, respectively, and two limestone samples show $\delta^{13}C_{PDB}$ = –0.03‰ to +0.3‰ and $\delta^{18}O_{SMOW}$= +22.5‰ to +23.1‰, with average values of +0.1‰ and +22.8‰, respectively.

4.2 Characteristics of $\delta^{13}C_{PDB}$ against $\delta^{18}O_{SMOW}$ values

Fig. 4A shows plots of $\delta^{13}C_{PDB}$ against $\delta^{18}O_{SMOW}$ values from the four different formations in the

Shangsi Section, from which, three groups are easily identified: 1) The samples shown by blank triangles and gray circles are collected from the Wujiaping and Maokou formations. They fall in a field of $\delta^{13}C_{PDB}$= +2.7‰ to +4.9‰ and $\delta^{18}O_{SMOW}$= +21.1‰ to +26.2‰, with average values of +3.8‰ and +24‰. 2) The Dalong Formation samples shown by black squares are distributed in a field of $\delta^{13}C_{PDB}$= –2.0‰ to +2.3‰ and $\delta^{18}O_{SMOW}$= +12.6‰ to +25.4‰, with average values of +0.5‰ and +21.8‰, which are both lower than the values from the first group. 3) The distribution of the Chihsian Formation samples shown by gray diamonds is not well concentrated relative to the other samples. The Chihsian Formation samples can be further divided into two sub-groups: a) eight samples from the lower Chihsian Formation (four bioclastic limestone and four limestone with dolomite spots, see detail for the lithology and sample location in Figs. 2 and 4B) show $\delta^{13}C_{PDB}$= –0.3‰ to +2.2‰ and $\delta^{13}O_{SMOW}$= +24.5‰ to +27.8‰, with average values of +1.2‰ and +25.8‰, respectively, which are close to values for typical marine limestone; b) the rest of the samples of the Chihsian Formation show $\delta^{13}C_{PDB}$ = +2.4‰ to +4.8‰ and $\delta^{13}O_{SMOW}$= +21.2‰ to +26.9‰, with average values of +3.6‰ and +25.0‰, respectively, which are close to those of first group, containing the Wujiaping and Maokou formations.

Table 2 presents the average $\delta^{13}C_{PDB}$ and $\delta^{18}O_{SMOW}$ values of samples from different lithology groups in the Chihsian (except the eight samples from the lower Chihsian Formation), Wujiaping and Maokou formations, where the dominant lithology is carbonates. Their $\delta^{13}C_{PDB}$ values show strong positive anomalous values in common. From Table 2, we can see that limestone (LM) interbedded with laminated LM/siliceous rocks/cherts contain higher $\delta^{13}C_{PDB}$ values than bioclastic LM and LM with shale/asphaltene, whereas the situation for $\delta^{18}O_{SMOW}$ values is the opposite. This result illustrates that the negative biasing $\delta^{18}O_{SMOW}$ values and strong positive bias $\delta^{13}C_{PDB}$ values are more obvious in LM interbedded with laminated LM/siliceous rocks/cherts.

4.3 Possible hydrothermal events in the Permian Shangsi Section

Processes of increasing temperature, rising sea level, prosperous biological production and rapid burial of organic carbon could induce a positive biasing in $\delta^{13}C_{PDB}$ and a negative biasing in $\delta^{18}O_{SMOW}$, and vice versa (Yan Zhaobin et al., 2005). The lower Chihsian Formation layers with $\delta^{13}C_{PDB}$ and $\delta^{18}O_{SMOW}$ values close to the typical marine limestone may hint a stable environment for this period, with a normal biological production/burial rate. However, characteristics of the negative biasing $\delta^{18}O_{SMOW}$ values and strong positive biasing $\delta^{13}C_{PDB}$ values from the middle-upper Chihsian, Wujiaping, and Maokou formations may indicate prosperous biological productivity with rapid burial of organic carbon during these periods and help to explain the general formation of laminated limestone and limestone interbedded with biogenic cherts/siliceous rocks.

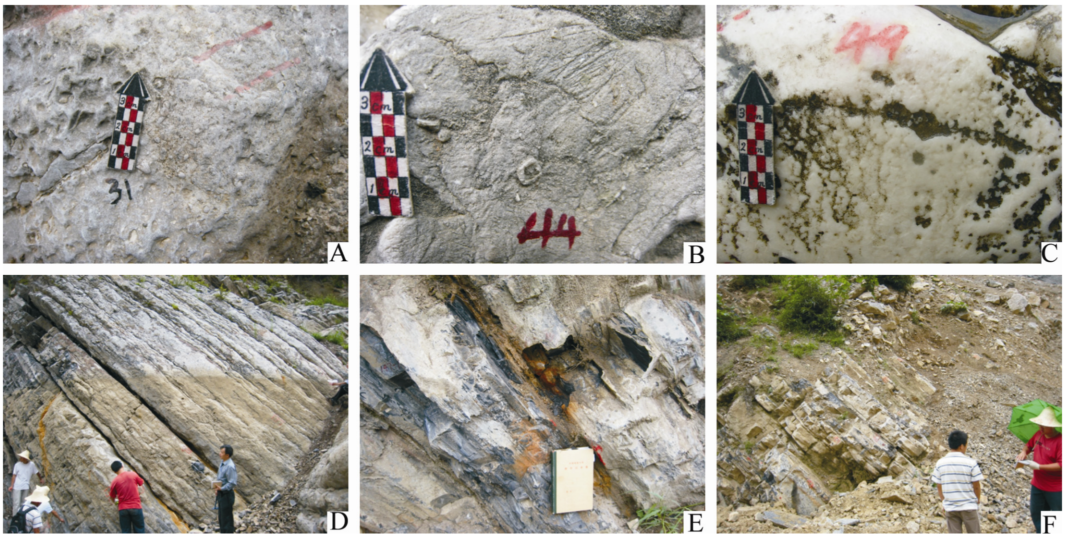

Fig. 3. Outcrop photographs for (A) gray thick-bedded bioclastic limestone and grainstone in Layer 31 (~67 m) of the Shangsi Section; (B) gray thick-bedded limestone, with plaque structure in Layer 44 (~107 m) of the Shangsi Section; (C) gray thick-bedded grain-phyric limestone in Layer 49 (~124 m) of the Shangsi Section; (D) gray mid-bedded limestone interbedded with dark thin-bedded limestone, and gray mid-/thick-bedded siliceous limestone, which consist of Layer 135 to 140 (~380 to ~385 m) of the Shangsi Section; (E) gray to dark gray mid-/thin-bedded limestone interbedded with volcanic ashes, which consist of Layer 145 to 149 (~392 to ~394 m) of the Shangsi Section; (F) dark thin-bedded siliceous rock interbedded with dark calcareous shale (referred as Ca-Shale in Fig. 4), which consist of Layer 159 to 164 (~410 to ~415 m) of the Shangsi Section.

Table 1 Lithologies and carbon and oxygen isotope composition of samples from the Shangsi Section in the Northwest Sichuan Basin, Southwest China

Formation	Layer	Thickness	Lithology	$\delta^{13}C_{PDB}$	$\delta^{18}O_{PDB}$	$\delta^{18}O_{SMOW}$
DL	164	415.53	SR	1.5700	-6.8500	23.8483
	160	410.95	SR interbedded with Ca-shale	1.1800	-5.3960	25.3472
	157	408.96	SR interbedded with C-shale	-0.0300	-8.2080	22.4483
	156	406.41	SR interbedded with Si-shale	0.9600	-7.2480	23.4380
	155	405.81	SR interbedded with Ca-shale	-1.0800	-17.8070	12.5526
	154	403.33	SR interbedded with Ca-shale & volcanic ash	1.2500	-9.9410	20.6617
	152	398.27	SR interbedded with Ca-shale	-1.9500	-9.4190	21.1999
	143	390.93	LM	0.3000	-7.5850	23.0905
	142	388.44	LM	2.8000	/	/
	140	386.80	LM	/	-3.9680	26.8193
	139	384.55	LM	/	-4.8230	25.9379
	135	378.96	Siliceous-LM interbedded with LM; Pyrite nodules	2.2500	-7.4680	23.2112
WJP	133	376.40	LM interbedded with cherts	3.1900	-4.8330	25.9276
	132	373.35	LM interbedded with siliceous clumps	3.5400	-5.7600	24.9720
WJP	131	369.75	LM interbedded with cherts	3.0700	-8.1850	22.4720
	130	367.55	LM interbedded with chert clumps	3.8500	-7.1580	23.5307
	129	363.84	LM interbedded with siliceous clumps	4.3600	-6.6110	24.0947
	127	357.78	LM interbedded with siliceous belts	4.9300	-6.3340	24.3802
	126	354.50	LM interbedded with siliceous clumps	4.6000	-6.8570	23.8411
	125	348.90	LM interbedded with cherts & siliceous lenses	3.6900	-5.2050	25.5441
	122	344.00	LM interbedded with siliceous clumps	4.2300	-6.2600	24.4565
	120	339.03	LM interbedded with cherts	4.4300	-8.5820	22.0627
	119	336.45	LM interbedded with siliceous clumps & mudstone	4.6900	-6.7830	23.9173
	118	331.45	LM interbedded with cherts	4.4000	-6.7860	23.9142
	117	329.30	LM interbedded with siliceous belts	3.8600	-6.5930	24.1132
	115	326.85	LM interbedded with chert clumps	2.7300	-7.0200	23.6730
MK	107	320.20	LM interbedded with Ca-shale & siliceous belts	2.8700	-6.7200	23.9823
	106	318.40	LM interbedded with Ca-shale & siliceous belts	3.7000	-7.4300	23.2503
MK	105	316.80	LM interbedded with Ca-shale	3.3700	-5.8500	24.8792
	104	315.02	LM interbedded with Ca-shale	2.8800	-5.8430	24.8864
	102	313.70	LM interbedded with Ca-shale & SR	3.5700	-9.1680	21.4586
	101	313.02	LM interbedded with Ca-shale & mudstone & siliceous belts	3.5800	-4.5720	26.1967
	100	311.80	LM interbedded with Ca-shale & siliceous belts/nodules	3.6200	-5.7650	24.9668
	99	310.10	LM interbedded with mudstone & siliceous belts	4.0250	-8.6500	21.9926
	97	307.30	LM interbedded with Ca-shale & siliceous nodules	3.1950	-8.2500	22.4050
	95	304.30	LM interbedded with Ca-shale & cherts	3.7200	-6.0400	24.6833
	94	299.90	LM containing with chert belts/nodules	4.4800	-6.6600	24.0441
	93	295.80	LM	3.6200	-5.0830	25.6699
	92	294.40	LM	4.2300	-7.1420	23.5472
	90	281.70	LM	4.0000	-9.4950	21.1215
	89	276.00	LM	4.2600	-6.5000	24.2091
	87	268.70	LM interbedded with siliceous belts & cherts	3.9600	-6.6110	24.0947
MK	86	264.20	LM interbedded with cherts	4.0750	-6.3000	24.4153
QX	85	257.00	LM; laminated/nodular LM	4.2275	-5.9400	24.7864
	84	245.10	LM interbedded with laminated/nodular limestone	4.8000	-7.3690	23.3132
	83	241.00	LM interbedded with laminated/nodular limestone	4.5950	-6.6100	24.0957
	82	235.30	LM interbedded with laminated LM	4.2300	-8.1360	22.5225
	81	232.40	LM interbedded with laminated LM	4.1400	-4.7360	26.0276
	77	216.90	LM	4.2000	-7.1720	23.5163
	76	214.90	LM; Nodular limestone	4.1500	-5.0350	25.7194
	75	205.00	LM	4.3400	-5.4750	25.2658
	74	200.20	LM interbedded with laminated LM	3.3050	-4.5100	26.2606
	73	197.10	Laminated LM interbedded with LM lenses	4.4050	-5.9100	24.8173
	72	193.50	LM; Lenticular limestone; Nodular limestone	4.1770	-4.2500	26.5286
	71	188.50	LM interbedded with shale	3.5200	-3.8720	26.9183
	70	184.50	LM interbedded with C-shale	3.1625	-5.4900	25.2503
	69	181.00	LM containing bitumen	3.0200	-4.9090	25.8493
QX	68	177.50	LM containing bitumen	2.4275	-7.4900	23.1885
	66	172.00	LM	3.6050	-7.0400	23.6524
	65	166.80	Laminated LM interbedded with LM lenses	3.5000	-6.5840	24.1225
	64	163.30	LM	3.4800	-5.7330	24.9998
	63	162.20	C-Laminated LM interbedded with LM lenses	3.9075	-5.9300	24.7967
	62	151.70	Laminated LM interbedded with LM lenses	3.8060	-5.1800	25.5699
	61	149.50	Laminated LM interbedded with LM lenses	3.5500	-5.6900	25.0441
	60	148.10	LM interbedded with lenses; See bitumen	4.1300	-4.3140	26.4627
	59	147.10	Bioclastic LM	3.8700	-4.2600	26.5183
	58	142.10	Bioclastic LM	3.4950	-4.3000	26.4771
	57	139.90	Bioclastic LM	3.0600	-5.3900	25.3534
	55	135.10	LM interbedded with laminated LM	3.8100	-3.9190	26.8699
	54	132.40	Laminated LM interbedded with LM	3.6600	-9.4020	21.2174
	53	130.30	Bioclastic LM	3.0000	-6.6350	24.0699
QX	52	129.50	LM interbedded with laminated LM; See bitumen	2.7600	-4.0160	26.7699
	51	127.10	Laminated LM with Ca-nodules	2.8400	-4.6400	26.1266
	49	126.23	Graniphyric LM	1.7100	-4.8200	25.9410
	44	110.03	LM with plaque structure	2.2300	-5.1430	25.6080
	39	93.03	Bioclastic LM	0.3600	-6.2330	24.4843
	35	81.33	Graniphyric LM	0.2100	-6.1600	24.5596
	31	68.73	Bioclastic LM; Grained LM	1.7000	-5.5020	25.2379
	30	65.58	Bioclastic LM	3.4950	-7.7300	22.9411
	29	61.58	Bioclastic LM	3.5200	-8.4720	22.1761
	27	56.48	Bioclastic LM	3.3800	-8.6680	21.9741
	25	50.08	Bioclastic LM	2.7000	-4.5290	26.2410
	23	45.98	Bioclastic LM	2.7000	-4.9990	25.7565
	21	42.60	Bioclastic LM interbedded with LM	2.8400	-4.7700	25.9926
	18	37.70	Bioclastic LM	1.7200	-4.9000	25.8585
QX	14	31.95	Bioclastic LM; Pyrite nodules	1.5600	-3.0040	27.8131
	13	30.45	LM with dolomite spots	-0.2900	-4.2740	26.5039

Thickness in m; isotopes in ‰; LM. limestone; SR. siliceous rock; Ca-. Calcareous; C-. Carbonaceous; Si-. Siliceous; DL. Dalong Formation; WJP. Wujiaping Formation; MK. Maokou Formation; QX. Qixia (Chihsian) Formation

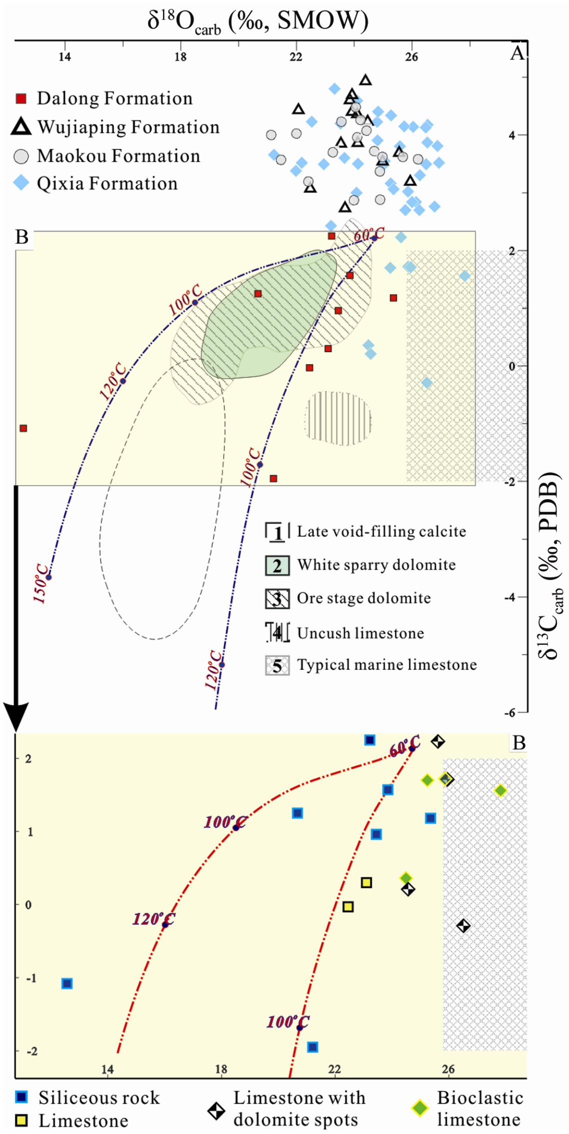

Fig. 4. $\delta^{13}C_{PDB}$ vs. $\delta^{18}O_{SMOW}$ for the Shangsi Section samples; the dashed curves in blue (A) and in red (B) represent the theoretical temperature curves. Sample symbols: 1. Late void-filling calcite; 2. white sparry dolomite; 3. ore stage dolomite; 4. uncush limestone (Spangenberg et al., 1996); 5. typical marine limestone, with $\delta^{13}C_{PDB}$ = 0‰ ±2‰ (Hoefs, 1997) and $\delta^{18}O_{SMOW}$ > +25.8‰ for confirming minor alteration influence (Derry et al., 1992); Ca-. calcareous.

Previous work on other South China Permian Sections connected the obvious negative biasing $\delta^{13}C_{PDB}$ values in the Late Permian strata to a mass biological extinction near the Permian-Triassic boundary (Gao Zhengang et al., 1987; Li Zishun et al., 1986; Huang Sijing et al., 1992). When compared with the $\delta^{13}C_{PDB}$ vs. $\delta^{18}O_{SMOW}$ graph for calcites from the San Vicente mine (Spangenberg et al., 1996), however, we found that plots of $\delta^{13}C_{PDB}$ vs. $\delta^{18}O_{SMOW}$ for samples from the Dalong Formation (black squares) were distributed close to the theoretical curves for calcite precipitated during mixing of fluids. A maximum temperature of ~100℃ could be inferred, which leads us to consider that the carbon and oxygen isotope characteristics in the Late Permian Dalong Formation of the Shangsi Section may not be the direct result of a mass biological extinction. In addition, volcanic ashes interbedded within strata have been observed from the Late Permian Dalong Formation (Table 1 and Fig. 3E). The ash confirms the existence of volcanic activities during the Late Permian in this area, which is in accordance with previous publications (Feng Shaonan, 1991; He Li et al., 2008; Niu Zhijun et al., 2000; Tian Shugang, 1991). Furthermore, Chen Hui et al. (2012) has discussed the hydrothermal contribution to the Late Permian Dalong Formation sediments indicated by geochemical characteristics of major and trace elements (which seem to not be classic hydrothermal deposits). The possible temperature inferred from this study during major hydrothermal deposition may not exceed 100℃ (Fig. 4). We suggest that negative biasing in both $\delta^{13}C_{PDB}$ and $\delta^{18}O_{SMOW}$ values in the Dalong Formation may reflect the influence of igneous/magmatic systems ($\delta^{13}C_{PDB}$= -3‰ to -30‰, $\delta^{18}O_{SMOW}$= +6‰ to +12‰) or the mantle origin ($\delta^{13}C_{PDB}$= -5‰ to -7‰) (Hoefs, 1997), on the depositions through hydrothermal events.

Table 2 Value ranges and average values of $\delta^{13}C_{PDB}$ vs. $\delta^{18}O_{SMOW}$ for different lithology groups from the Chihsian, Maokou and Wujiaping formations (except the 8 samples from the lower Chihsian Formation)

Host rock	Value range	Average value
	$\delta^{13}C_{PDB}$ (‰)	
LM with laminated LM	2.8–4.8	4.0
LM	3.5–4.3	4.0
LM with siliceous rock	2.9–4.9	3.9
LM with chert	2.7–4.5	3.8
LM with shale	2.6–3.9	3.3
Bioclastic LM	2.7–3.9	3.2
LM with asphaltene	2.4–3.0	2.7
	$\delta^{18}O_{SMOW}$ (‰)	
LM with laminated LM	21.2–26.9	24.7
LM	21.1–26.5	24.6
LM with siliceous rock	21.5–26.2	23.9
LM with chert	22.1–25.9	24.0
LM with shale	24.9–26.9	25.4
Bioclastic LM	22.0–26.5	24.8
LM with asphaltene	23.2–26.8	25.3

Note: LM=Limestone.

5 Conclusions

Combined carbon and oxygen isotope measurements of the Permian Shangsi Section and suggest following results,

(1) Samples from the underlying Permian Wujiaping, Maokou, and middle-upper Chihsian formations with negative biasing $\delta^{18}O_{SMOW}$ values and strong positive anomalous $\delta^{13}C_{PDB}$ values indicate prosperous biological productivity and rapid burial of organic carbon.

(2) Samples with both negative anomalous $\delta^{13}C_{PDB}$ and $\delta^{18}O_{SMOW}$ values from the Dalong Formation reveal minor contribution of hydrothermal processes, with the possible temperature <100℃.

Acknowledgements This study was financially supported by the Key Project of the Natural Science Foundation of Hubei Province (2008CDA095) and the SINOPEC project (G0800-06-ZS-319). We appreciate the collaboration with and support from Prof. Xie Shucheng and Prof. Yan Jiaxin.

References

Bai Xiao, Luo Genming, Wu Xia, Wang Youzhen, Huang Junhua, and Wang Xinjun (2008) Carbon isotope records indicative of paleoceanographical events at the latest Permian Dalong Formation at Shangsi, Northeast Sichuan, China [J]. *Journal of China University of Geosciences*. **19**, 481–487.

Chen Hui, Xie Xinong, Hu Chaoyong, Huang Junhua, and Li Hongjing (2012) Geochemical characteristics of Late Permian sediments in the Dalong Formation of the Shangsi Section, Northwest Sichuan Basin in South China [J]. *Journal of Geochemical Exploration*. **112**, 35–53.

Coplen T.B., Kendall C., and Hopple J. (1983) Comparison of stable isotope reference samples [J]. *Nature*. **302**, 236–238.

Derry L.A., Kaufman A.J., and Jacobsen S.B. (1992) Sedimentary cycling and environmental change in the Late Proterozoic: Evidence from stable and radiogenic isotopes [J]. *Geochimica et Cosmochimica Acta*. **56**, 1317–1329.

Feng Shaonan (1991) New knowledge on Dongu Movement [J]. *Geoscience*. **5**, 378–384 (in Chinese).

Gao Zhengang, Xu Daoyi, Zhang Qinwen, and Sun Yiyin (1987) Discovery and study of microspherules at the Permian-Triassic boundary of the Shangsi Section, Guangyuan, Sichuan [J]. *Geological Review*. **33**, 203–211 (in Chinese).

Ghazban F., Schwarcz H.P., and Ford D.C. (1991) Stable isotopic composition of the hydrothermal fluids responsible for the Nanisivik Zn-Pb deposits, Northwest-Territories, Canada [J]. *Applied Geochemistry*. **6**, 257–266.

Hao Fang, Guo Tonglou, Zhu Yangming, Cai Xunyu, Zou Huayao, and Li Pingping (2008) Evidence for multiple stages of oil cracking and thermochemical sulfate reduction in the Puguang Gas Field, Sichuan Basin, China [J]. *AAPG Bulletin*. **92**, 611–637.

He Li, Luo Xiao, Liu Liping, Li Ping, and Zhou Guixiang (2008) A discussion on depositional environment in Late Permian and distribution of reef-bank in Sichuan Basin [J]. *Natural Gas Industry*. **28**, 28–32 (in Chinese).

Hu Guoyi, Wang Weisheng, and Liao Fengrong (2012) Geochemical characteristics and its influencing factors of light hydrocarbon in coal-derived gas: A case study of Sichuan Basin [J]. *Acta Petrologica Sinica*. **28**, 905–916 (in Chinese).

Huang Sijing (1992) Clay minerals in clay rocks near P/T boundary from Guangyuan, Sichuan and Chongqing [J]. *Journal of Chengdu College of Geology*. **19**, 66–73 (in Chinese).

Huang Zhilong, Li Xiaobao, Zhou Meifu, Li Wenbo, and Jin Zhongguo (2010) REE and C-O isotopic geochemistry of calcites from the world-class Huize Pb-Zn deposits, Yunnan, China: Implications for the ore genesis [J]. *Acta Geologica Sinica-English Edition*. **84**, 597–613.

Hoefs J. (1997) *Stable Isotope Geochemistry* [M]. Springer Verlag, Berlin.

Isozaki Y., Shimizu N., Yao Jianxin, Ji Zhansheng, and Matsuda T. (2007) End-Permian extinction and volcanism induced environmental Stress: the Permian-Triassic boundary interval of lower-slope facies at Chaotian, South China [J]. *Palaeogeography, Palaeoclimatology, Palaeoecology*. **252**, 218–238.

Lai Xulong, Wang Wei, Wignall P.B., Bond D.G., Jiang Haishui, Ali J.R., John E.H., and Sun Yadong (2008) Palaeoenvironmental change during the end-Guadalupian (Permian) mass extinction in Sichuan, China [J]. *Palaeogeography, Palaeoclimatology, Palaeoecology*. **269**, 78–93.

Li Pengwei, Huang Junhua, Chen Min, and Bai Xiao (2009) Coincident negative shifts in sulfur and carbon isotope compositions prior to the end-Permian mass extinction at Shangsi Section of Guangyuan, South China [J]. *Frontiers of Earth Science in China*. **3**, 51–56.

Li Zishun, Zhan Lipei, Zhu Xiufang, Zhang Jinghua, Jin Ruogu, Liu Guifang, Sheng Huaibin, Shen Guimei, Dai Jinye, Huang Hengquan, Xie Longchun, and Yan Zheng (1986) Mass extinction and geological events between Palaeozoic and Mesozoic Era [J]. *Acta Geologica Sinica*. **62**, 1–17 (in Chinese).

Ma Yongsheng (2008) Geochemical characteristics and origin of natural gases from Puguang gas field on eastern Sichuan Basin [J]. *Natural Gas Geoscience*. **19**, 1–6 (in Chinese).

Ma Zhixin, Yan Jiaxin, Xie Xinong, Ruan Xiaoyan, and Li Bo (2008) Depositional and ecological features of Permian oxygen deficient deposits at Shangsi Section, Northeast Sichuan, China [J]. *Journal of China University of Geosciences*. **19**, 488–495.

Ma Zhongwu, Hu Chaoyong, Yan Jiaxin, and Xie Xinong (2008) Biogeochemical records at Shangsi Section, Northeast Sichuan in China: The Permian paleoproductivity proxies [J]. *Journal of China University of Geosciences*. **19**, 461–470.

Niu Zhijun, Duan Qifa, Xu Guanghong, and Xu Anwu (2000) Sedimentation types and age of the Dalong Formation in Western Hubei [J]. *Journal of Stratigraphy*. **24**, 151–155 (in Chinese).

Qi Liang, Wang C.Y., and Zhou Meifu (2008) Controls on the PGE distribution of Permian Emeishan alkaline and peralkaline volcanic rocks in Longzhoushan, Sichuan Province, SW China [J]. *Lithos*. **106**, 222–236.

Rao Dan, Qin Jianzhong, Tenger, and Zhang Meizhen (2008) Source analysis of oil seepage and bitumen originating from marine layer strata in Guangyuan area, the Northwest Sichuan Basin [J]. *Petroleum Geology & Experiment*. **30**, 596–605 (in Chinese).

Ruan Xiaoyan, Luo Genming, Hu Shouzhi, Chen Feng, Sun Si, Wu Wenjun, Guo Qiaozhen, and Liu Guoquan (2008) Molecular records of primary producers and sedimentary environmental conditions of Late Permian rocks in Northeast Sichuan, China [J]. *Journal of China University of Geosciences*. **19**, 471–480.

Spangenberg J., Fontbote L., Sharp Z.D., and Hunziker J. (1996) Carbon and oxygen isotope study of hydrothermal carbonates in the zinc-lead deposits of the San Vicente district, central Peru: A quantitative modeling on mixing processes and CO_2 degassing [J]. *Chemical Geology*. **133**, 289–315.

Tao Shizhen, Dai Jinxing, Zhou Caineng, Wang Jinghong, Mi Jinggui, Wang Zecheng, and Hu Suyun (2012) The trace of genesis, formation and mineral resources of natural gas and rare gas isotope existing in volcanic inclusion of Songliao Basin [J]. *Acta Petrological Sinica*. **28**, 927–938 (in Chinese).

Tian Shugang (1991) The terrestrial cause of organic extinction by the end of Permian [J]. *Acta Geosicientia Sinica*. **12**, 167–178 (in Chinese).

Wang Yigang, Wen Yingchu, Hong Haitao, Xia Maolong, Zhang Jing, Song Shuyun, and Liu Huayi (2006) Petroleum geological characteristics of deep water deposits in Upper Permian-Lower Triassic trough in Sichuan Basin and adjacent areas [J]. *Oil & Gas Geology*. **27**, 702–714 (in Chinese).

Xie Xinong, Li Hongjing, Xiong Xiang, Huang Junhua, Yan Jiaxin, Qin Jianzhong, Tenger, and Li Wu (2008) Main controlling factors of organic matter richness in a Permian section of Guanyuan, Northeast Sichuan [J]. *Journal of China University of Geosciences*. **19**, 507–517.

Xu Sihuang and Watney W.L. (2007) Dominant factors in controlling marine gas pools in South China [J]. *Frontiers of Earth Science in China*. **1**, 491–497.

Yan Jiaxin, Ma Zhixin, Xie Xinong, Xue Wuqiang, Li Bo, and Liu Dongqin (2008) Subdivision of Permian fossil communities and habitat types in Northeast Sichuan, South China [J]. *Journal of China University of Geosciences*. **19**, 441–450.

Yan Zhaobin, Guo Fusheng, Pan Jiayong, Guo Guolin, and Zhang Yuejing (2005) Application of C, O and Sr isotope composition of carbonates in the research of paleoclimate and paleooceanic environment [J]. *Contributions to Geology and Mineral Resources Research*. **20**, 53–56 (in Chinese).

Yang Rongjun, Liu Shugen, and Wu Xichun (2009) Preliminary discussion on bank and reef facies characteristics of Ma'antang Formation in West Sichuan Province and the oil-gas potential [J]. *Contributions to Geology and Mineral Resources Research*. **24**, 73–76 (in Chinese).

Yin Hongfu, Zhang Kexin, Tong Jinnan, Yang Zunyi, and Wu Shunbao (2001) The global stratotype section and point (GSSP) of the Permian-Triassic Boundary [J]. *China Basic Science*. **3**, 12–25 (in Chinese).

Zhang Bing, Zheng Rongcai, Wang Xuben, Zheng Chao, Wen Huaguo, Luo Yuan, and Chi Yuelong (2012) Geochemical characteristics and diagenetic systems of dolomite reservoirs of the Changxing Formation in the eastern Sichuan Basin, China [J]. *Petroleum Science*. **9**, 141–153.

Zhang Qu, Tenger, Meng Qingqiang, Qin Jianzhong, Jiang Qigui, and Zheng Lunju (2008) Genesis of marine carbonate natural gas in the northeastern Sichuan Basin, China [J]. *Acta Geological Sinica—English Edition*. **82**, 577–584.

Zhou Huayao, Hao Fang, Li Pingping, and Zhang Xuefeng (2008) Source rocks for the giant Puguang Gas Field, Sichuan Basin: Implication for petroleum exploration in marine sequences in South China [J]. *Acta Geological Sinica—English Edition*. **82**, 477–486.

Zhou Lian, Zhang Haiqiang, Wan Jin, Huang Junhua, and Xie Xinong (2008) Assessment on redox conditions and organic burial of siliciferous sediments at the latest Permian Dalong Formation in Shangsi, Sichuan, South China [J]. *Journal of China University of Geosciences*. **19**, 496–506.

Zhu Guangyou, Zhang Shuichang, Huang Haiping, Liang Yingbo, Meng Shucui, and Li Yuegang (2011) Gas genetic type and origin of hydrogen sulfide in the Zhongba gas field of the western Sichuan Basin, China [J]. *Applied Geochemistry*. **26**, 1261–1273.

Zhu Yangming, Li Ying, Hao Fang, Zou Huayao, and Guo Tonglou (2008) Compositional characteristics and origin of marine and terrestrial solid reservoir bitumen in the Northeast Sichuan Basin [J]. *Acta Petrologica Sinica*. **28**, 870–878 (In Chinese).